Open Ceramics 5 (2021) 100065

Contents lists available at ScienceDirect

Open Ceramics

journal homepage: www.editorialmanager.com/oceram

Factors influencing thermal conductivity and compressive strength of natural fiber-reinforced geopolymer foams

Katharina Walbrück [a,*], Lisabeth Drewler [a], Steffen Witzleben [a], Dietmar Stephan [b]

[a] Department of Natural Sciences, Bonn-Rhine-Sieg University of Applied Sciences, von-Liebig-Str. 20, 53359, Rheinbach, Germany
[b] Building Materials and Construction Chemistry, Department of Civil Engineering, Technische Universität Berlin, Gustav-Meyer-Allee 25, 13355, Berlin, Germany

ARTICLE INFO

Keywords:
Geopolymer
Foaming
Fiber reinforcement
Miscanthus
Thermal conductivity
Compressive strength

ABSTRACT

New sustainable, environmentally friendly materials for thermal insulation of buildings are necessary to reduce their carbon footprints. In this study, *Miscanthus* fiber-reinforced geopolymer composites, foamed with sodium dodecyl sulfate (SDS), were developed using fly ash as a geopolymer precursor. The effects of fiber content, fiber size, curing temperature, foaming agent content, fumed silica specific surface area and fumed silica content on thermal conductivity and compressive strength were evaluated using a Plackett-Burman design of experiment. Furthermore, the microstructure of geopolymer composites was investigated using X-ray diffraction (XRD), X-ray micro-computed tomography (μCT) and scanning electron microscopy (SEM). The measured characteristic values were in the following ranges: Thermal conductivity 0.057 W (m K)$^{-1}$ to 0.127 W (m K)$^{-1}$, compressive strength 0.007 MPa–0.719 MPa and porosity 49 vol% to 76 vol%. The results reveal an enhancement of thermal conductivity by elevated fiber size and foaming agent content. In contrast, the compressive strength is enhanced by high fiber content. Additionally, SEM images indicate a good interaction between the fibers and the geopolymer matrix, because nearly the whole fiber surface is covered by the geopolymer.

1. Introduction

A variety of thermal insulation materials is available on the European market. About 60% of the market is dominated by mineral or inorganic fibrous materials like glass and stone wool, 30% by organic foamy materials (expanded polystyrene, extruded polystyrene and polyurethane) and 10% account for combined materials (wool-wool, gypsum-foam) and new technology materials like nano-cellular-foams or transparent materials [1]. However, due to the energy consumption during the production and the use of non-renewable materials, thermal insulations cause significant adverse effects on the environment. Especially in respect of the advancing climate change, limited fossil resources and the global energy demand, the reduction of energy consumption of buildings is one of the most important challenges of the 20th century. Therefore, the development of sustainable thermal insulation materials based on renewable resources and industrial waste are becoming more attractive [2,3].

Very promising groups of renewable resources with numerous advantages are fast-growing low input grasses such as *Miscanthus*. *Miscanthus*, which is originates from (sub) tropical regions in Asia, is a perennial rhizomatous sweet grass (Poaceae) with a C_4 photosynthetic pathway [4]. Due to the remarkable adaptability to a wide range of environmental conditions, *Miscanthus* is suitable for establishment and distribution under European climatic conditions. Currently, the genus *Miscanthus* includes approximately 17 species, especially; *Miscanthus sinensis*, *Miscanthus sacchariflorus, Miscanthus floridulus* and *Miscanthus x giganteus* have received much attention in Europe. The genotype *Miscanthus x giganteus* is a triploid hybrid between the diploid *Miscanthus sinensis* and the tetraploid *Miscanthus sacchariflorus*. [5–9] Due to its C_4 photosynthetic pathway, *Miscanthus* is extremely efficient in CO_2 capture and storage. Unlike C_3 plants such as rice, C_4 plants are able to fix CO_2 into the four-carbon (C_4) compounds malate and aspartate [8–13]. Beside the increased photosynthesis activity, *Miscanthus* possesses several further advantages such as low density, low thermal conductivity, high biomass yield and low greenhouse gas emissions [4,14,15].

In the context of advancing climate change, irresponsible waste management is besides increasing CO_2 emissions, one of the significant problems. Cement is the most essential binding material in the world but releases a vast amount of CO_2 during production. Nowadays, by partially replacing it with industrial waste like fly ash, metakaolin, silica fume, steel slag and zeolite, the usage of cement can be minimized. However, in order to reduce greenhouse gas emissions, the demand for sustainable, eco-friendly building materials is growing. Aluminosilicate polymers, so-

* Corresponding author.
E-mail address: katharina.walbrueck@h-brs.de (K. Walbrück).

https://doi.org/10.1016/j.oceram.2021.100065
Received 4 December 2020; Received in revised form 26 January 2021; Accepted 27 January 2021
Available online 31 January 2021

Table 1
Considered factors for the DOE and their high and low levels.

Factor	Lower level		Higher limit	
Fiber content	30	wt%	40	wt%
Fiber size	125–250	µm	250–500	µm
Foaming agent content	0.2	wt%	0.4	wt%
Curing temperature	50	°C	70	°C
Fumed silica specific surface area	90	$m^2\ g^{-1}$	200	$m^2\ g^{-1}$
Fumed silica content	1.0	wt%	3.0	wt%

called geopolymers, offers a novel way to produce sustainable, environmentally friendly building materials. In principle, these are two-component systems consisting of an aluminosilicate source and an alkaline activator, usually an alkali metal silicate or hydroxide. The most commonly used aluminosilicate components are fly ash (FA), granulated blast-furnace slag (GGBFS) or metakaolin (MK). The three-dimensional aluminosilicate network consists of cross-linked aluminate and silicate tetrahedrons, whose negative charge is balanced by the incorporation of alkali cations such as Na^+ or K^+ [16–25].

In order to combine the advantages of foam concrete and geopolymers, recent innovations in the field of geopolymers, are focused on the development of geopolymer foams for thermal insulation. The production of geopolymer foams is done either by chemical or mechanical foaming or through the formation of syntactic foams. In the chemical foaming method, the voids are generated after adding aluminum powder or hydrogen peroxide as a result of a gas releasing reaction. In comparison, mechanical foaming is either performed by mixing a pre-made foam with the geopolymer slurry or during the mixing process after adding a surfactant. The third method for the production of geopolymer foams is the formation of syntactic foams. Hereto, hollow spheres like cenospheres, hollow glass micro-balls or hollow polymeric microspheres are embedded into the binding matrix [20,21,26–29]. In the present study, geopolymer foams reinforced with *Miscanthus x giganteus* fibers are synthesized, and the effects of fiber content, fiber size, foaming agent content, curing temperature, fumed silica specific surface area and fumed silica content is investigated using Plackett-Burman design to find the optimum thermal conductivity and compressive strength.

1.1. Design of experiments

In the field of research and production, experiments are often conducted aiming at optimizing a specific process. This optimum can depend on various parameters and it can be measured by one or more properties. Conventional approaches to find this optimum are trial and error or changing one factor at a time. For complex problems with a great number of influencing variables, they have proven to be ineffective, regarding time, costs and resources [30–32]. Design of experiments (DoE) is a systematic approach for product and process optimization using statistical models, allowing understanding of how variables influence the result. One of its advantages is testing multiple factors simultaneously, thus minimizing the number of experiments required and making it an efficient tool [31,33,34]. The DoE consists of two phases, screening and optimizing: During factor screening, the most significant input variables affecting the result of the experiment are identified. The aim is to reduce the number of parameters demanding further investigation. These most crucial influencing factors are further investigated in the following optimization experiments to provide more details on the relationship between the factors and the output variables [33,35]. Several different types of experimental designs find application such as Bayesian experimental design, block design, Box–Behnken design, central composite design, fractional factorial design, optimal design, Plackett-Burman design, Latin squares or Taguchi methods [30,32,36,37]. In this present investigation, Plackett-Burman design using Minitab software is applied. It is a two-level multifactorial design, meaning all influencing factors are varied on a low and a high value. This method was selected because it determines crucial factors as well as interactions using as few experimental runs as possible [31,33,36]. Other possible design methods often used for screening are 2-level fractional factorial design, supersaturated design and definitive screening design [31,33].

2. Material and methods

2.1. Materials

In order to prepare sustainable, environmentally friendly foamed

Table 3
Effects and P-values of the factors for thermal conductivity.

Source	Effect	P-Value	Significance
Constant		0.000	
Fiber content	0.13470	0.073	significant
Fiber size	−0.02990	0.004	significant
Foaming agent content	−0.02577	0.008	significant
Curing temperature	−0.00870	0.204	not significant
Fumed silica specific surface area	−0.00970	0.164	not significant
Fumed silica content	0.00970	0.164	not significant

Table 4
Effects and P-values of the factors for compressive strength.

Source	Effect	p-Value	Significance
Constant		0.015	
Fiber content	0.2246	0.094	significant
Fiber size	−0.3142	0.038	significant
Foaming agent content	−0.2474	0.074	significant
Curing temperature	−0.0304	0.782	not significant
Fumed silica specific surface area	−0.0744	0.509	not significant
Fumed silica content	0.0856	0.451	not significant

Table 2
Mixture design combinations for natural fiber-reinforced geopolymer foam concrete.

Combination	Fiber content	Fiber size	Foaming agent content	Curing temperature	Fumed silica specific surface area	Fumed silica content
	[wt%]	[µm]	[wt%]	[°C]	[$m^2\ g^{-1}$]	[wt%]
S1	40	125	0.2	70	90	1
S2	40	250	0.4	50	90	1
S3	30	250	0.2	70	90	3
S4	40	125	0.4	70	200	1
S5	40	250	0.4	50	90	3
S6	40	250	0.2	70	200	3
S7	30	250	0.4	70	200	1
S8	30	125	0.4	70	90	3
S9	30	125	0.4	50	200	3
S10	40	125	0.2	50	200	3
S11	30	250	0.2	50	200	1
S12	30	125	0.2	50	90	1

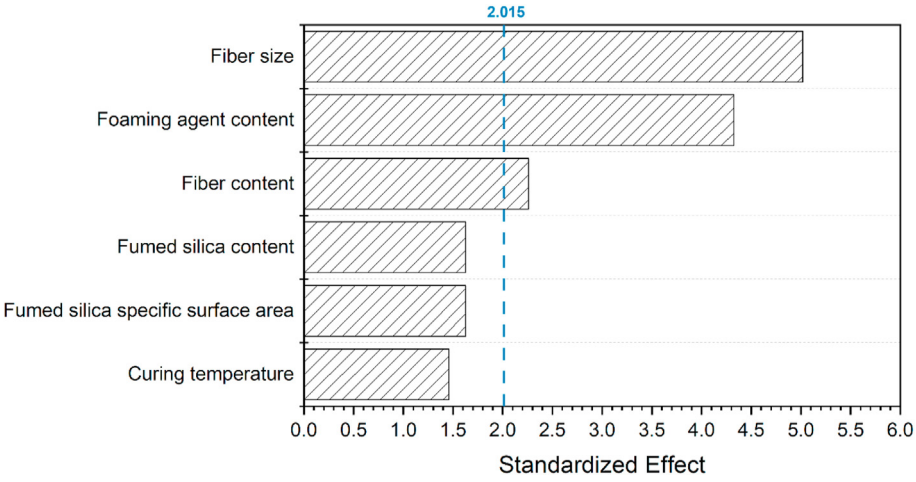

Fig. 1. Pareto plot of the standardized effects for thermal conductivity (α = 0.1).

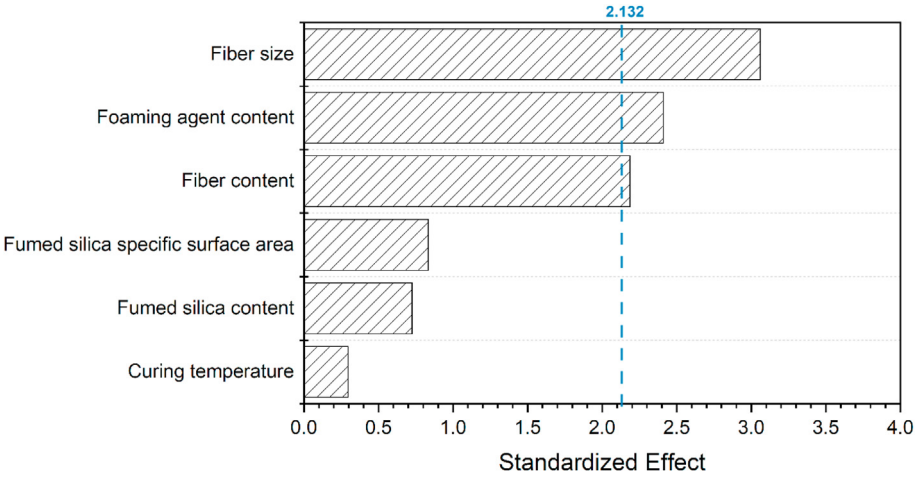

Fig. 2. Pareto plot of the standardized effects for compressive strength (α = 0.1).

Table 5
Thermal conductivity and compressive strength.

Sample	Thermal conductivity W (m K)$^{-1}$	Compressive strength MPa
S1	0.127 ± 0.011	0.719 ± 0.023
S2	0.062 ± 0.004	0.017 ± 0.002
S3	0.062 ± 0.002	0.018 ± 0.004
S4	0.091 ± 0.023	0.390 ± 0.173
S5	0.062 ± 0.003	0.007 ± 0.001
S6	0.079 ± 0.004	0.196 ± 0.019
S7	0.060 ± 0.001	n.r.[a]
S8	0.057 ± 0.003	0.021 ± 0.004
S9	0.093 ± 0.013	0.174 ± 0.035
S10	0.121 ± 0.008	0.676 ± 0.032
S11	0.088 ± 0.006	0.272 ± 0.018
S12	0.103 ± 0.018	0.193 ± 0.021

[a] n. r. = no result.

geopolymer composites, fly ash (FA), sodium silicate, *Miscanthus x giganteus*, sodium dodecyl sulfate (SDS) and fumed silica nanoparticles are used. The fly ash with the commercial name EFA-Füller® HP is supplied by BauMineral GmbH, Germany. Sodium silicate with a composition of 28.50 wt% SiO_2 and 8.29 wt% Na_2O is obtained from Carl Roth GmbH + Co. KG, Germany. The *Miscanthus x giganteus* was cultivated in 2012 at the field lab Campus Klein-Altendorf (University of Bonn, Germany) and harvested in April 2018. The dry biomass was milled using a BHS 100 (Buschhoff) hammer mill equipped with a 1.1 mm sieve (University of Bonn). As foaming agent sodium dodecyl sulfate (SDS), from Carl Roth, is used. The fumed silica nanoparticles Aerosil® 90 and Aerosil® 200 (Evonik Industries AG, Germany) are used as a foam stabilizer.

2.2. Experimental design

The geopolymer experiments were performed using design of experiments (DoE) as a tool to evaluate the effects of fiber content, fiber size, foaming agent content, curing temperature, specific surface area of fumed silica and fumed silica content on thermal conductivity and compressive strength of the natural fiber-reinforced geopolymer foams. The DoE used was a Plackett-Burman design, consisting of six factors and 12 experiments (N = 12), as presented in Table 2. The six factors considered in this study are summarized in Table 1, including their high and low levels. The selection of the high and low levels were based on preliminary tests and through a review of relevant literature [21,38]. The responses analyzed were thermal conductivity and compressive strength. The results were assessed by analysis of variances (ANOVA) and Pareto diagram with Minitab 18 (Minitab, Inc., USA) to verify the factors displaying a significance higher then 10%.

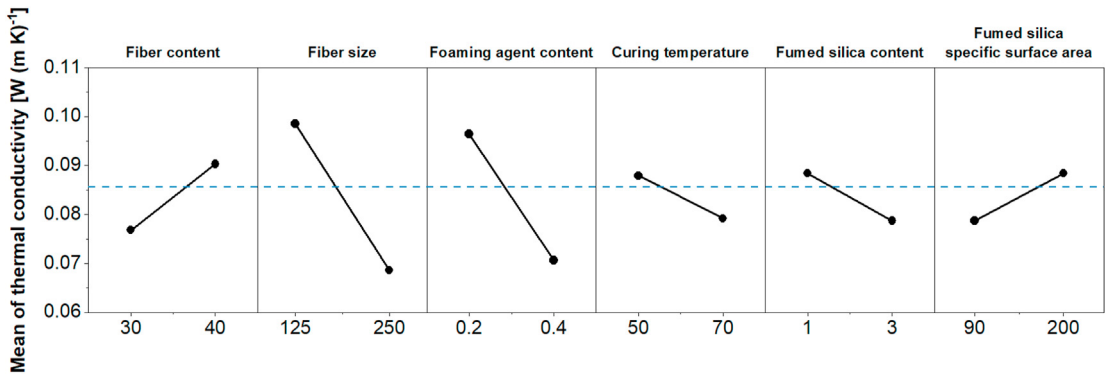

Fig. 3. Main effects plot for thermal conductivity.

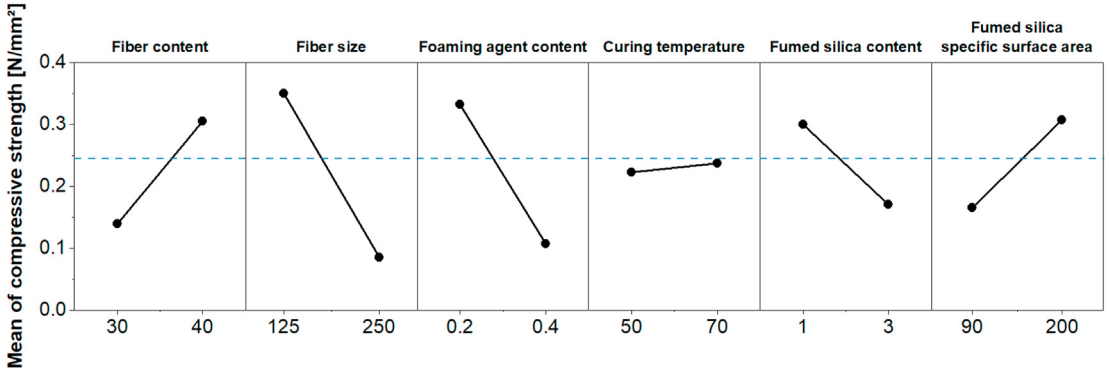

Fig. 4. Main effects plot for compressive strength.

Table 6
Total porosity of the samples obtained by micro tomography.

Sample	S1	S2	S3	S4	S5	S6	S7	S8	S9	S10	S11	S12
Total porosity (vol%)	49.6	72.8	67.6	57.1	75.9	71.8	71.0	67.8	63.2	45.9	62.3	53.6

2.3. Synthesis of natural fiber-reinforced geopolymer foams

Foam geopolymer concrete was prepared, by activating a dry mix of fly ash, *Miscanthus x giganteus,* sodium dodecyl sulfate and fumed silica (specific surface area 90 $m^2\ g^{-1}$ or 200 $m^2\ g^{-1}$) with an alkaline solution. The alkaline solution is a mixture of 64 wt% sodium silicate solution and 36 wt% water. The slurry was stirred at high speed (speed position 2 of the mixer) for 5 min using a Hobart N50 mortar mixer. Afterwards, the resultant mixture was poured into a 40 × 40 × 160 mm^3 triplet steel mold for X-ray diffraction, X-ray micro-computed tomography and scanning electron microscopy tests, and in 140 × 140 × 40 mm^3 steel molds for thermal conductivity and compressive strength tests. The samples were cured at 50 °C/70 °C and ambient pressure for 48 h and afterwards at room temperature until 28 d.

2.4. Characterization

Characterization of the geopolymer foam concrete was carried out using thermal conductivity tests, compressive strength, X-ray micro-computed tomography (μCT), X-ray diffraction (XRD) and scanning electron microscopy (SEM).

2.4.1. Thermal conductivity

The thermal conductivity of the 140 × 140 × 40 mm^3 specimens was measured by using a heat flow meter apparatus (HFM 446 Lambda Small, Netzsch, Germany). Two external thermocouples were placed in the center on the front and back side of the specimens with aluminum adhesive tape. Three samples of each formulation were measured and for each sample, at least six measurements were performed to ensure reproducibility.

2.4.2. Compressive strength

A Z010 universal strength testing apparatus (1 kN and 10 kN capacity, Zwick/Roell, Germany) with a testing speed of 2 mm min^{-1} was used to determine the compressive strength. The samples (140 × 140 × 40 mm^3) were cut to a size of 60 × 60 × 40 mm^3 and the compressive strength was measured at 10% deformation. Each measurement was carried out four times.

2.4.3. X-ray micro-computed tomography

X-ray micro-computed tomography (μCT) was used to determine the porosity of natural fiber-reinforced geopolymer foam concrete. The μCT measurements were performed using SkyScan 1275 (Bruker) with a micro focus X-ray tube (100 kV and 100 μA) and a flat-panel detector. The samples (40 × 40 × 160 mm^3) were cut with a diamond hole saw to create a cylinder with a diameter of 20 mm. The cylindrical samples were scanned over a 360° interval with a rotation step of 0.5° and a resolution of 14 μm.

2.4.4. X-ray diffraction

X-ray diffraction (XRD) analysis was performed using a D2 Phaser X-ray diffractometer (Bruker AXS) with a Cu Kα radiation source (30 kV

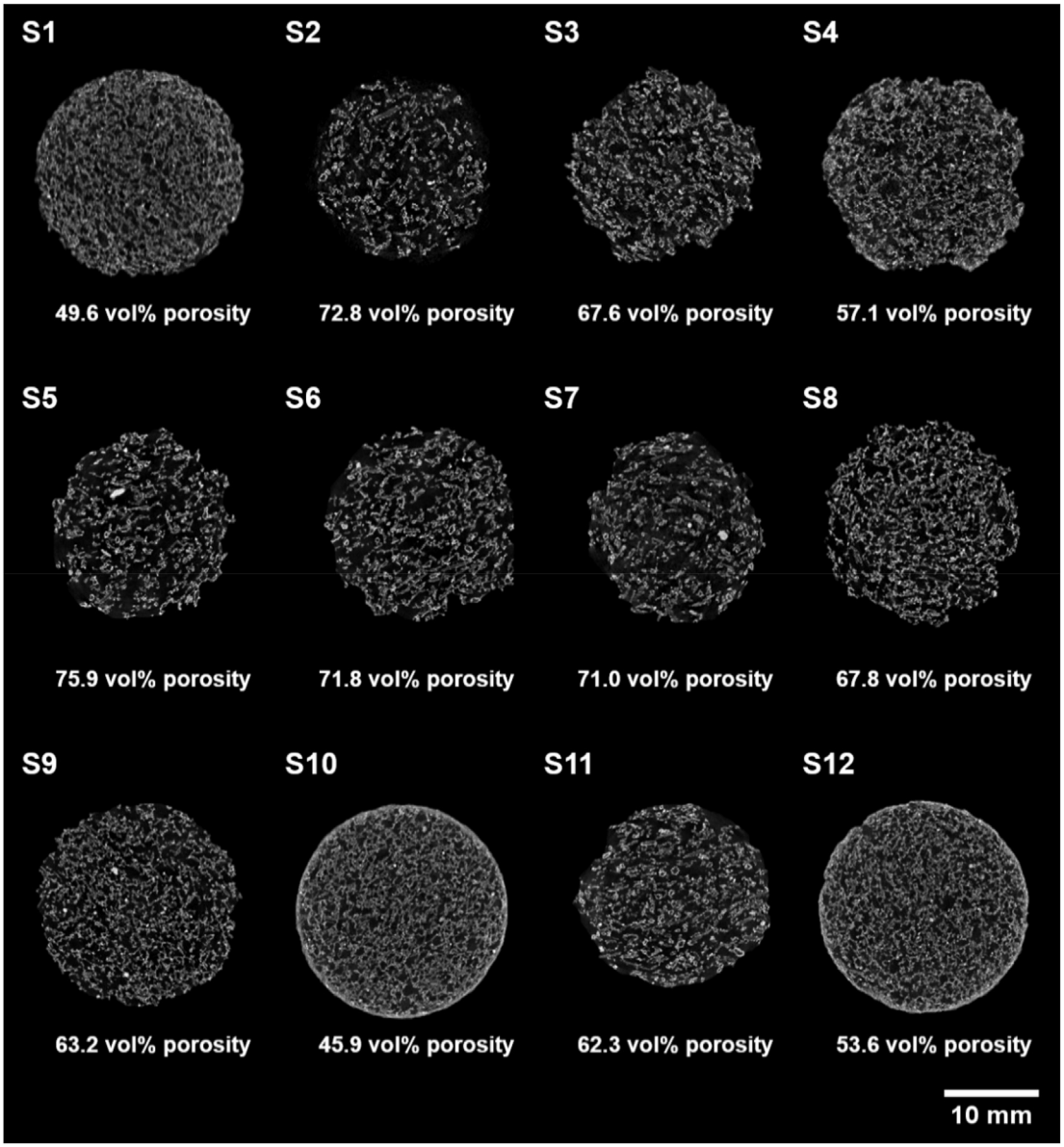

Fig. 5. μ-CT cross-sectional images.

and 10 mA) and a LynxEye detector. The powder patterns are collected in the 2θ range 10°–65° with a step size of 0.01° and a time of 2.0 s step^{-1}. The samples were prepared by grinding and mixing 600 mg of the geopolymer powder (<63 μm) with 20 mg of Lanthanum hexaboride (LaB_6, Sigma-Aldrich) as an internal standard. The use of an internal standard allows the determination of the crystalline and amorphous content. Diffrac. Eva and Diffrac. Topas software from Bruker were used for phase identification and Rietveld refinement.

2.4.5. Scanning electron microscopy (SEM)

The surface morphology of the foamed geopolymer concrete was investigated using a field emission scanning electron microscope JSM-7200 F (JEOL). For the observation, the specimens were cut into small pieces and were mounted on a bulk sample holder.

3. Results and discussion

3.1. Design of experiments

Analysis of variance (ANOVA) on thermal conductivity and compressive strength of *Miscanthus* fiber-reinforced geopolymer foams was used to determine the optimum level of the considered factors. As shown in Tables 3 and 4, the fiber content, fiber size and foaming agent content have the highest negative and positive effect on both thermal conductivity and compressive strength. Furthermore, the P-value gives information about the influence level of the different input parameters on the response variable. A P-value less than $\alpha = 0.1$ indicates an input parameter with a significant influence. Thereby, both responses are significantly influenced by the input parameters fiber size, foaming agent content and fiber content. However, the other facts do not influence the both responses.

To support the findings, the Pareto plot of the standardized effects in Figs. 1 and 2 compare the significance of each effect. Any factor that extends past the blue reference line is potentially important. For both response variables, thermal conductivity and compressive strength, the Pareto plot shows that the factors fiber size, foaming agent content and fiber content are significant. However, the factors curing temperature, fumed silica specific surface area and fumed silica content are not significant for thermal conductivity and compressive strength.

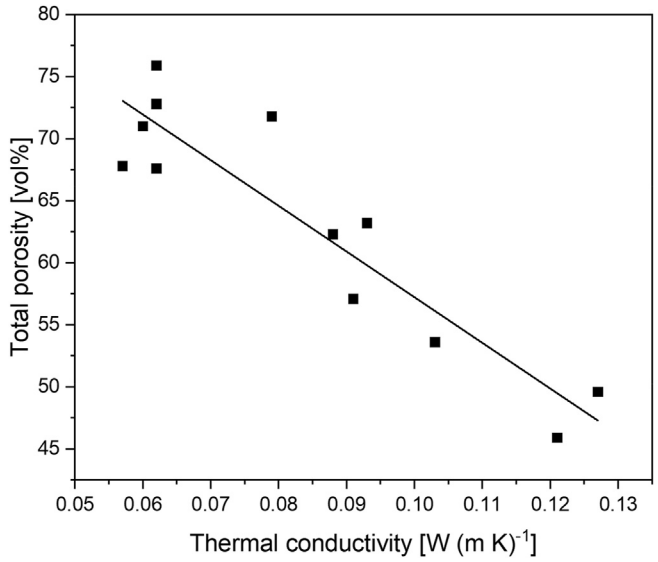

Fig. 6. Relationship between total porosity and thermal conductivity.

3.2. Thermal conductivity

The values for the thermal conductivity of all geopolymer samples are presented in Table 5. Here sample S8 exhibits with 0.057 ± 0.003 W (m K)$^{-1}$ the smallest and sample S1 with 0.127 ± 0.011 W (m K)$^{-1}$ the highest thermal conductivity. Furthermore, to understand the effects of the six input variables on the thermal conductivity, Fig. 3 represents the main effects plot. By plotting the means of the thermal conductivity at each level of the factor, it can be inferred that with an increase in fiber content, fiber size and foaming agent the thermal conductivity decreases. Whereas no significant influence on the thermal conductivity was observed regarding the variables curing temperature, fumed silica content and fumed silica specific surface area.

The increase of fiber size from 125 to 250 μm leads to a reduction in thermal conductivity from 0.0985 to 0.0686 W (m K)$^{-1}$. The reasons for the reduction in thermal conductivity are attributed to the packing of the fibers within the geopolymer matrix and the core-shell structure of *Miscanthus*. Firstly, the less dense packing of larger fibers leads to more air voids and therefore to lower thermal conductivity. Secondly, as reported by Chen et al. larger *Miscanthus* fibers exhibit, due to the core-shell structure, a higher amount of parenchyma and, therefore, a higher porosity [14]. *Miscanthus* fibers are made up of an outer shell, the so-called epidermis, and the core structure, composed of sclerenchyma, radial allocation of vascular bundles and porous parenchyma, which is responsible for the low thermal conductivity of the fibers [14,39,40].

Besides the fiber size, also the amount of foaming agent added shows a significant influence on the thermal conductivity. The different amounts of foaming agent lead to a change in the density and porosity of the fiber-reinforced geopolymer foams, which are important factors affecting the thermal conductivity. Therefore, the increase of foaming agent from 0.2 to 0.4 wt% leads to a reduction in thermal conductivity from 0.964 to 0.071 W (m K)$^{-1}$.

3.3. Compressive strength

The compressive strength values, as shown in Table 5, were determined at the curing age of 28 d. Sample S1 exhibits with 0.719 MPa, the highest, and sample S5 with 0.007 MPa, the lowest compressive strength. Furthermore, the influence of fiber content, fiber size, foaming agent content, curing temperature, fumed silica content, and specific surface area of fumed silica on the compressive strength of *Miscanthus* fiber-reinforced geopolymer foams are displayed in Fig. 4. An increased amount of *Miscanthus* fibers from 30 to 40 wt% leads to a significant increase in the strength from 0.139 to 0.305 MPa. Shah et al. investigated geopolymer composites reinforced with basalt, steel and polyvinyl alcohol (PVA) fibers in a low concentration range of 0.5–2 wt%. They observed for PVA and basalt fibers an increase in compressive strength with increasing fiber content. However, this behavior could not be observed for steel fibers. The highest compressive strength for steel fibers was achieved at 1 wt%. According to Shah et al. two phenomena can be observed in respect of compressive strength due to the addition of fibers. They reported that an increase in compressive strength can be observed when the capacity of the fibers to prevent cracks overshadows the effect of the induced porosity through the fibers. In contrast, a decrease in compressive strength can be observed when the increase in porosity dominates [41]. Alomayri and Low investigated geopolymer composites

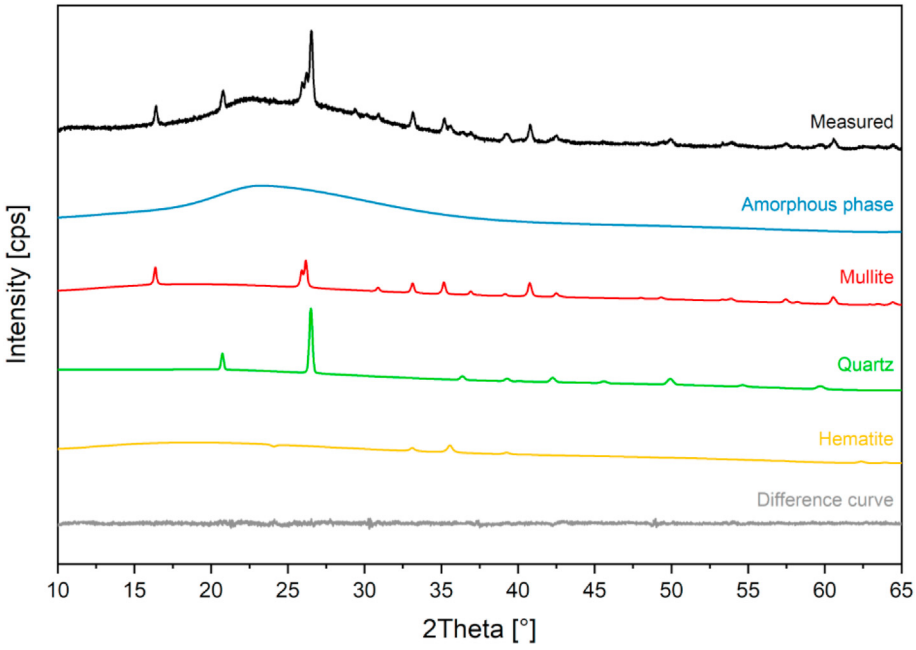

Fig. 7. XRD Rietveld refinement for sample S1.

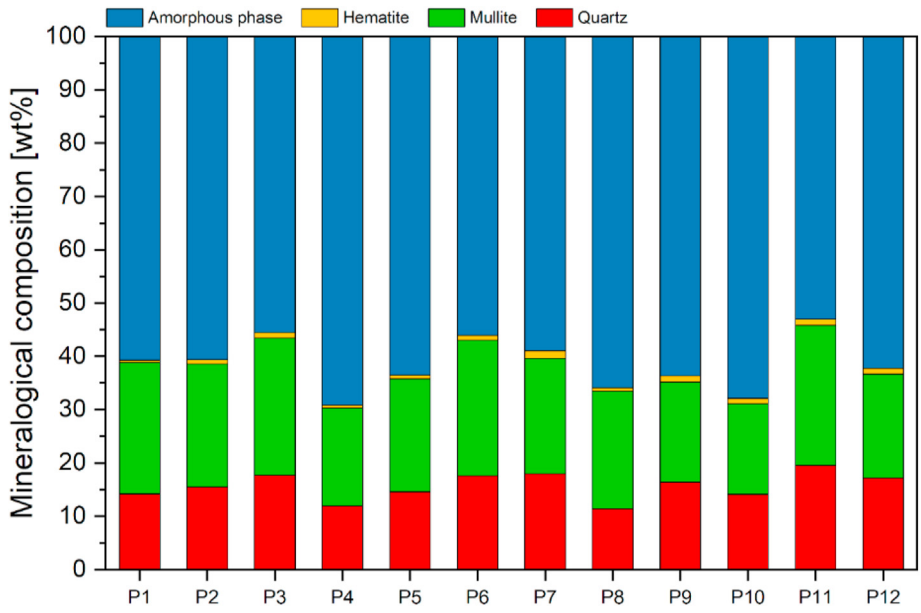

Fig. 8. Mineralogical composition of the samples determined by Rietveld refinement.

Table 7
Mineralogical composition of the samples determined by Rietveld refinement.

Sample	Quartz [wt %]	Mullite [wt %]	Hematite [wt %]	Amorphous phase [wt %]
S1	14.2 ± 2.0	24.6 ± 2.2	0.4 ± 0.3	60.8 ± 1.0
S2	15.5 ± 0.3	23.1 ± 0.7	0.8 ± 0.1	60.6 ± 1.0
S3	17.7 ± 2.2	25.7 ± 0.8	1.1 ± 0.2	55.5 ± 2.2
S4	12.0 ± 1.6	18.4 ± 2.5	0.5 ± 0.1	69.2 ± 3.5
S5	14.6 ± 1.0	21.2 ± 1.4	0.7 ± 0.1	63.5 ± 2.3
S6	17.6 ± 0.8	25.4 ± 1.5	0.9 ± 0.2	56.1 ± 2.3
S7	17.9 ± 2.4	21.7 ± 4.0	1.4 ± 0.3	59.0 ± 6.7
S8	11.4 ± 1.8	22.0 ± 2.5	0.7 ± 0.2	65.9 ± 4.1
S9	16.4 ± 1.5	18.8 ± 3.6	1.2 ± 0.2	63.7 ± 5.0
S10	14.1 ± 0.7	17.1 ± 0.9	0.9 ± 0.1	67.9 ± 1.3
S11	19.5 ± 2 1	26.3 ± 4.3	1.1 ± 0.1	53.0 ± 3.3
S12	17.2 ± 3.7	19.5 ± 1.8	1.1 ± 0.1	62.3 ± 2.8

reinforced with different amounts of cotton fibers (0–1 wt%). They reported that geopolymer composites reinforced with 0.5 wt% cotton had the highest compressive strength. Alomayri and Low attributed this behavior to the fiber-reinforcement of the geopolymers; thereby, higher loads are transferred from the geopolymer matrix to the *Miscanthus* fibers. Furthermore, they reported a good dispersion of cotton fibers within the matrix leads to an increase fiber-matrix adhesion [42]. The different fibers and fiber content makes it difficult to compare the results. However, the results of Shah et al. [41] for the PVA and basalt fibers show a similar trend. Besides the fiber content, also the fiber size and the amount of added foaming agent show a significant influence on the compressive strength. Comparable to the results for the thermal conductivity, the increase of fiber size from 125 to 250 μm leads to a less dense packing and the higher amount of parenchyma of the fibers to a reduction in compressive strength from 0.350 to 0.085 MPa. Moreover, the increase of foaming agent from 0.2 to 0.4 wt% leads to a change in density and porosity to a reduction in compressive strength from 0.332 to 0.125 MPa.

3.4. X-ray micro-computed tomography

Quantitative analysis was performed using the Bruker CTAn image-analyzing program. The results concerning total porosity are given in Table 6 and Fig. 5. From Fig. 5, which provides two-dimensional cross-sections of each sample, it can be observed that the pores do not have a regular round shape, and they are inhomogeneously distributed over the sample. The reason for the irregular shape of the pores and the inhomogeneous distribution can possibly be attributed to the inhomogeneous pore structure of the *Miscanthus* parenchyma. From Table 6, it can be seen

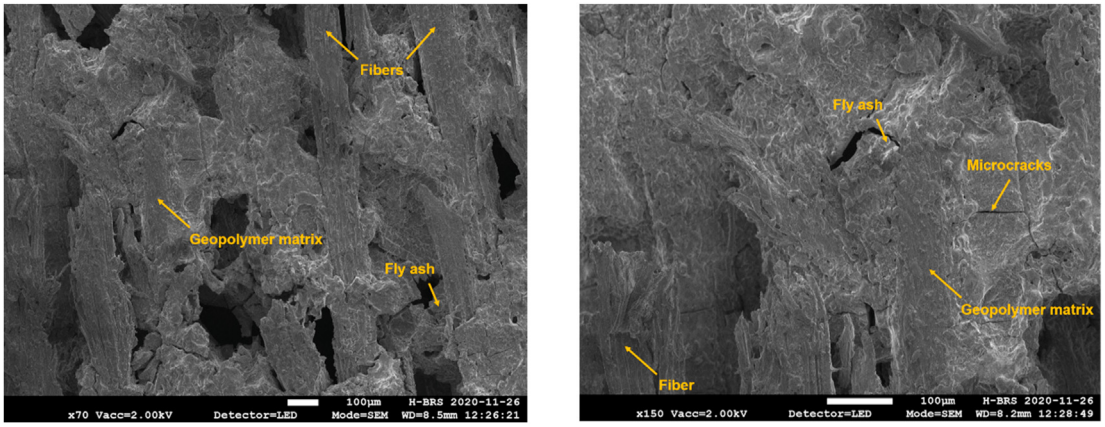

Fig. 9. SEM image of sample S10 with different magnification.

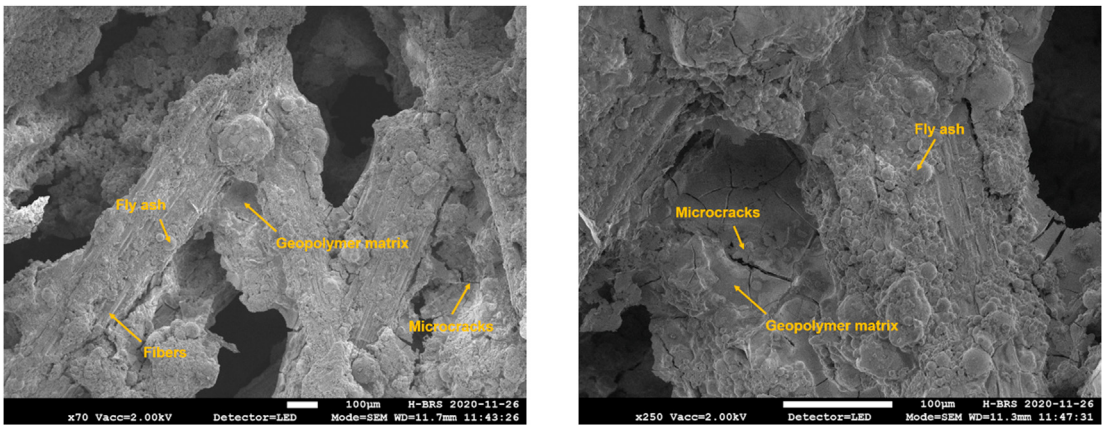

Fig. 10. SEM image of sample S5 with different magnification.

that the measured porosity ranges from 49 to 76 vol% of the total volume. Furthermore, the increase of foaming agent from 0.2 to 0.4 wt% leads to higher porosity and, therefore, as mentioned in chapter 2.2, to a reduction in thermal conductivity. In addition, the increase of fiber size from 125 to 250 µm leads to an increase in porosity and thermal conductivity.

It is a well-known fact that the porosity affects the thermal conductivity. Therefore, Fig. 6 shows the relationship between porosity and thermal conductivity. It can be observed that the highest porosity values are obtained in those samples that have the lowest thermal conductivity.

3.5. X-ray diffraction

Fig. 7 shows the results of the XRD analysis of the prepared geopolymer samples (cured for 28 d). The crystalline phases identified are quartz (COD 9005020), mullite (COD 7105575) and hematite (COD 1011267). In addition to the crystalline components, a broad peak in the region 16°–36° 2θ arise from the amorphous phase.

Quantitative X-ray diffraction analysis has shown that the prepared geopolymers are about 60% amorphous. The mineralogical composition for each sample determined by Rietveld refinement is listed in Fig. 8. Furthermore, the analysis of the mineralogical composition performed in triplicate revealed comparable results, as indicated by the standard deviation in Table 7. As can be seen from the results, the addition of 40 wt% fibers and smaller fibers increased the amorphous content. The growth of the amorphous content in the samples could be attributed to the amorphous nature of the *plant* fibers [43].

3.6. Scanning electron microscopy

Selected samples were investigated using SEM. The SEM images in Figs. 9 and 10 exhibit the surface of the geopolymer foam reinforced with *Miscanthus* fibers. In both cases, the images display a porous structure with fibers and unreacted fly ash particles embedded in the geopolymer matrix. The SEM images shows that the sample S10 (Fig. 9) hat a denser structure, compared to sample S5 (Fig. 5). However, for Sample S5 more micro cracks were present on the surface, which reduces the compressive strength and increases the porosity [44]. SEM investigations support the findings of the performed X-ray micro-computed tomography and the compressive strength measurements. Compared to sample S5, sample S10 exhibits a higher compressive strength and porosity. Additionally, the SEM investigations provide first information about the fiber-matrix interaction. The fiber surface appears to be almost completely covered by geopolymer; this indicates for both samples a good interaction between fibers and matrix. However, the fiber-matrix interaction was not futher investigated in this study.

4. Conclusions

In this study, the effects of six parameters, namely fiber content, fiber size, foaming agent content, curing temperature, fumed silica content, and fumed silica specific surface area on thermal conductivity and compressive strength of *Miscanthus* fiber-reinforced geopolymer foams was investigated. Analysis of variance (ANOVA) revealed the fiber content, fiber size and foaming agent content have significant effects on the thermal conductivity and compressive strength, whereas the curing temperature, fumed silica content and fumed silica specific surface area have no significant effect. According to the main effects plot, the optimal conditions for minimal thermal conductivity are 30 wt% fibers with a size of 250 µm and 0.4 wt% foaming agent. Whereas the optimal conditions for maximum compressive strength are 40 wt% fibers with a size of 125 µm and 0.2 wt% foaming agent. The findings of X-ray micro-computed tomography and the SEM investigations exhibit a significant relation between thermal conductivity, porosity, and crack formation. Additionally, good interaction between the fibers and the geopolymer matrix can be observed on the SEM images, because nearly the whole fiber surface is covered by the geopolymer. However, further investigation is needed to determine the fiber-matrix adhesion. Based on these observations, *Miscanthus* fiber-reinforced geopolymer foams represent a potential sustainable eco-friendly material for thermal insulation. Thus, future research should focus on the environmental impact of *Miscanthus* fiber-reinforced geopolymer foams.

Funding

This work was supported by the European Regional Development Fund [Grant No. EFRE 0500035] and the German Federal Ministry of Education and Research [Grant No. 13FH158IN6].

Declaration of competing interest

The authors declare that they have no known competing financial interests or personal relationships that could have appeared to influence the work reported in this paper.

Acknowledgments

The authors would like to thank F. Maeting (Bonn-Rhein-Sieg University of Applied Sciences, Germany) for assistance in sample preparation. C. Dresbach and R. Rech (Bonn-Rhein-Sieg University of Applied Sciences, Germany) for help with the compressive strength measurements and R. Pude, G. Völkering and L. Moll (INRES, University of Bonn, Germany) for providing the *Miscanthus* biomass.

References

[1] F. Ardente, M. Beccali, M. Cellura, M. Mistretta, Building energy performance: a LCA case study of kenaf-fibres insulation board, Energy Build. 40 (2008) 1–10, https://doi.org/10.1016/j.enbuild.2006.12.009.

[2] R. Muthuraj, C. Lacoste, P. Lacroix, A. Bergeret, Sustainable thermal insulation biocomposites from rice husk, wheat husk, wood fibers and textile waste fibers: elaboration and performances evaluation, Ind. Crop. Prod. 135 (2019) 238–245, https://doi.org/10.1016/j.indcrop.2019.04.053.

[3] F. Asdrubali, F. D'Alessandro, S. Schiavoni, A review of unconventional sustainable building insulation materials, Sustain. Mater. Technol. 4 (2015) 1–17, https://doi.org/10.1016/j.susmat.2015.05.002.

[4] I. Lewandowski, J.C. Clifton-Brown, J.M.O. Scurlock, W. Huisman, Miscanthus, European experience with a novel energy crop, Biomass Bioenergy 19 (2000) 209–227, https://doi.org/10.1016/S0961-9534(00)00032-5.

[5] M.S. Dwiyanti, A. Rudolph, K. Swaminathan, A. Nishiwaki, Y. Shimono, S. Kuwabara, H. Matuura, M. Nadir, S. Moose, J.R. Stewart, T. Yamada, Genetic analysis of putative triploid miscanthus hybrids and tetraploid M. Sacchariflorus collected from sympatric populations of kushima, Japan, Bioenergy Res 6 (2013) 486–493, https://doi.org/10.1007/s12155-012-9274-3.

[6] A. Kiesel, C. Nunn, Y. Iqbal, T. Van der Weijde, M. Wagner, M. Özgüven, I. Tarakanov, O. Kalinina, L.M. Trindade, J. Clifton-Brown, I. Lewandowski, Site-specific management of miscanthus genotypes for combustion and anaerobic digestion: a comparison of energy yields, Front. Plant Sci. 8 (2017) 1–15, https://doi.org/10.3389/fpls.2017.00347.

[7] N. Brosse, A. Dufour, X. Meng, Q. Sun, A. Ragauskas, Miscanthus : a fast-growing crop for biofuels and chemicals production, Biofuels, Bioprod. Biorefining. 6 (2012) 580–598, https://doi.org/10.1002/bbb.1353.

[8] J. Rumpf, X.T. Do, R. Burger, Y.B. Monakhova, M. Schulze, Extraction of high-purity lignins via catalyst-free organosolv pulping from low-input crops, Biomacromolecules 21 (2020) 1929–1942, https://doi.org/10.1021/acs.biomac.0c00123.

[9] M. Bergs, G. Völkering, T. Kraska, R. Pude, X.T. Do, P. Kusch, Y. Monakhova, C. Konow, M. Schulze, Miscanthus x giganteus stem versus leaf-derived lignins differing in monolignol ratio and linkage, Int. J. Mol. Sci. 20 (2019), https://doi.org/10.3390/ijms20051200.

[10] R.C. Leegood, C4 photosynthesis: principles of CO2 concentration and prospects for its introduction into C3 plants, J. Exp. Bot. 53 (2002) 581–590, https://doi.org/10.1093/jexbot/53.369.581.

[11] E.A. Kellogg, C4 photosynthesis, Curr. Biol. 23 (2013) 594–599, https://doi.org/10.1016/j.cub.2013.04.066.

[12] J.P. McCalmont, A. Hastings, N.P. McNamara, G.M. Richter, P. Robson, I.S. Donnison, J. Clifton-Brown, Environmental costs and benefits of growing Miscanthus for bioenergy in the UK, GCB Bioenergy 9 (2017) 489–507, https://doi.org/10.1111/gcbb.12294.

[13] J.A. Langdale, C 4 Cycles: past, present, and future research on C 4 photosynthesis, Plant Cell 23 (2011) 3879–3892, https://doi.org/10.1105/tpc.111.092098.

[14] Y.X. Chen, F. Wu, Q. Yu, H.J.H. Brouwers, Bio-based ultra-lightweight concrete applying miscanthus fibers: acoustic absorption and thermal insulation, Cement Concr. Compos. 114 (2020), https://doi.org/10.1016/j.cemconcomp.2020.103829.

[15] U. Jørgensen, Benefits versus risks of growing biofuel crops: the case of Miscanthus, Curr. Opin. Environ. Sustain. 3 (2011) 24–30, https://doi.org/10.1016/j.cosust.2010.12.003.

[16] S. Apithanyasai, N. Supakata, S. Papong, The potential of industrial waste: using foundry sand with fly ash and electric arc furnace slag for geopolymer brick production, Heliyon 6 (2020), e03697, https://doi.org/10.1016/j.heliyon.2020.e03697.

[17] N. Toniolo, A.R. Boccaccini, Fly ash-based geopolymers containing added silicate waste. A review, Ceram. Int. 43 (2017) 14545–14551, https://doi.org/10.1016/j.ceramint.2017.07.221.

[18] G. Iswarya, M. Beulah, Use of zeolite and industrial waste materials in high strength concrete – a review, Mater. Today Proc. (2020), https://doi.org/10.1016/j.matpr.2020.06.329. In press.

[19] S.S. Kumar, A. Kumar, S. Singh, S.K. Malyan, S. Baram, J. Sharma, R. Singh, A. Pugazhendhi, Industrial wastes: fly ash, steel slag and phosphogypsum- potential candidates to mitigate greenhouse gas emissions from paddy fields, Chemosphere 241 (2020) 124824, https://doi.org/10.1016/j.chemosphere.2019.124824.

[20] Z. Zhang, J.L. Provis, A. Reid, H. Wang, Geopolymer foam concrete: an emerging material for sustainable construction, Construct. Build. Mater. 56 (2014) 113–127, https://doi.org/10.1016/j.conbuildmat.2014.01.081.

[21] K. Walbrück, F. Maeting, S. Witzleben, D. Stephan, Natural fiber-stabilized geopolymer foams-A review, Materials 13 (2020), https://doi.org/10.3390/ma13143198.

[22] J.L. Provis, J.S.J. Van Deventer, Introduction to geopolymers, in: Geopolymers, Elsevier, 2009, pp. 1–11, https://doi.org/10.1533/9781845696382.1.

[23] J. Davidovits, Geopolymers - inorganic polymeric new materials, J. Therm. Anal. 37 (1991) 1633–1656, https://doi.org/10.1007/BF01912193.

[24] P. Duxson, J.L. Provis, Designing precursors for geopolymer cements, J. Am. Ceram. Soc. 91 (2008) 3864–3869, https://doi.org/10.1111/j.1551-2916.2008.02787.x.

[25] P. Duxson, A. Fernández-Jiménez, J.L. Provis, G.C. Lukey, A. Palomo, J.S.J. Van Deventer, Geopolymer technology: the current state of the art, J. Mater. Sci. 42 (2007) 2917–2933, https://doi.org/10.1007/s10853-006-0637-z.

[26] V. Ducman, L. Korat, Characterization of geopolymer fly-ash based foams obtained with the addition of Al powder or H2O2 as foaming agents, Mater. Char. 113 (2016) 207–213, https://doi.org/10.1016/j.matchar.2016.01.019.

[27] A. Hajimohammadi, T. Ngo, P. Mendis, J. Sanjayan, Regulating the chemical foaming reaction to control the porosity of geopolymer foams, Mater. Des. 120 (2017) 255–265, https://doi.org/10.1016/j.matdes.2017.02.026.

[28] L. Zhang, F. Zhang, M. Liu, X. Hu, Novel sustainable geopolymer based syntactic foams: an eco-friendly alternative to polymer based syntactic foams, Chem. Eng. J. 313 (2017) 74–82, https://doi.org/10.1016/j.cej.2016.12.046.

[29] A. Hajimohammadi, T. Ngo, J.L. Provis, T. Kim, J. Vongsvivut, High strength/density ratio in a syntactic foam made from one-part mix geopolymer and cenospheres, Compos. B Eng. 173 (2019) 106908, https://doi.org/10.1016/j.compositesb.2019.106908.

[30] M. Ben Chobba, M. Messaoud, J. Bouaziz, F. De Leo, C. Urzì, The Effect of Heat Treatment on Photocatalytic Performance and Antibacterial Activity of TiO2 Nanoparticles Prepared by Sol-Gel Method, 2020, https://doi.org/10.1007/978-3-030-24247-3_9.

[31] M. Abhilash, S. Jhanjhari, P. Parthiban, J. Karthikeyan, Axial behaviour of semi-lightweight aggregate concrete-filled steel tube columns - a DOE approach, J. Constr. Steel Res. 162 (2019) 105614, https://doi.org/10.1016/j.jcsr.2019.05.004.

[32] N. Alagumurthi, K. Palaniradja, V. Soundararajan, Optimization of grinding process through Design of Experiment (DOE) - a comparative study, Mater. Manuf. Process. 21 (2006) 19–21, https://doi.org/10.1080/AMP-200060605.

[33] R. Ghanem, H. Owhadi, D. Higdon, Handbook of Uncertainty Quantification, Springer International Publishing, Switzerland, 2017, https://doi.org/10.1007/978-3-319-12385-1.

[34] R. Ruby-Figueroa, Design of experiment (DOE), in: Encycl. Membr, Springer-Verlag, Berlin, Heidelberg, 2016, pp. 533–535, https://doi.org/10.1007/978-3-662-44324-8.

[35] J. Antony, Screening Designs, Elsevier Ltd, 2014, https://doi.org/10.1016/b978-0-08-099417-8.00005-5.

[36] V.P. Astkahov, J.C. Outeiro, Finite element modelling, in: Machining. Fundamentals and Recent Advances, Springer International Publishing, Switzerland, 2008.

[37] R. Mohebi, K. Behfarnia, M. Shojaei, Abrasion resistance of alkali-activated slag concrete designed by Taguchi method, Construct. Build. Mater. 98 (2015) 792–798, https://doi.org/10.1016/j.conbuildmat.2015.08.128.

[38] K. Walbrück, S. Witzleben, D. Stephan, Neuartige Geopolymer-gebundene Dämmstoffe aus nachwachsenden Rohstoffen, in: Tagung Bauchemie, 2019, p. 500035, https://doi.org/10.13140/RG.2.2.27126.75844.

[39] R. Pude, C.H. Treseler, R. Trettin, G. Noga, Suitability of Miscanthus genotypes for lightweight concrete, Bodenkultur 56 (2005) 61–69.

[40] P. Klímek, R. Wimmer, P. Meinlschmidt, J. Kúdela, Utilizing Miscanthus stalks as raw material for particleboards, Ind. Crop. Prod. 111 (2018) 270–276, https://doi.org/10.1016/j.indcrop.2017.10.032.

[41] S.F.A. Shah, B. Chen, S.Y. Oderji, M. Aminul Haque, M.R. Ahmad, Comparative study on the effect of fiber type and content on the performance of one-part alkali-activated mortar, Construct. Build. Mater. 243 (2020) 118221, https://doi.org/10.1016/j.conbuildmat.2020.118221.

[42] T. Alomayri, I.M. Low, Synthesis and characterization of mechanical properties in cotton fiber-reinforced geopolymer composites, J. Asian Ceram. Soc. 1 (2013) 30–34, https://doi.org/10.1016/j.jascer.2013.01.002.

[43] X. Li, L.G. Tabil, S. Panigrahi, Chemical treatments of natural fiber for use in natural fiber-reinforced composites: a review, J. Polym. Environ. 15 (2007) 25–33, https://doi.org/10.1007/s10924-006-0042-3.

[44] M.M. Al Bakri Abdullah, K. Hussin, M. Bnhussain, K.N. Ismail, Z. Yahya, R.A. Razak, Fly ash-based geopolymer lightweight concrete using foaming agent, Int. J. Mol. Sci. 13 (2012) 7186–7198, https://doi.org/10.3390/ijms13067186.